# Homogentisic acid induces morphological and mechanical aberration of ochronotic cartilage in alkaptonuria

Journal of Cellular Physiology

# Homogentisic acid induces morphological and mechanical aberration of ochronotic cartilage in alkaptonuria

| | |
|---|---|
| Journal: | *Journal of Cellular Physiology* |
| Manuscript ID | JCP-18-1041.R1 |
| Wiley - Manuscript type: | Original Research Article |
| Date Submitted by the Author: | n/a |
| Complete List of Authors: | Bernardini, Giulia; Università degli Studi di Siena, Dipartimento di Biotecnologie, Chimica e Farmacia<br>Leone, Gemma; Università degli Studi di Siena, Dipartimento di Biotecnologie, Chimica e Farmacia<br>Millucci, Lia; Università degli Studi di Siena, Dipartimento di Biotecnologie, Chimica e Farmacia<br>Consumi, Marco; Università degli Studi di Siena, Dipartimento di Biotecnologie, Chimica e Farmacia<br>Braconi, Daniela; Università degli Studi di Siena<br>Spiga, Ottavia; Università degli Studi di Siena, Dipartimento di Biotecnologie, Chimica e Farmacia<br>Galderisi, Silvia; Università degli Studi di Siena, Dipartimento di Biotecnologie, Chimica e Farmacia<br>Marzocchi, Barbara; Università degli Studi di Siena, Dipartimento di Biotecnologie, Chimica e Farmacia; Azienda Ospedaliera Universitaria Senese, UOC Patologia Clinica<br>Viti, Cecilia; Università degli Studi di Siena, Dipartimento di Scienze Fisiche, della Terra e dell'Ambiente<br>Giorgetti, Giovanna; Università degli Studi di Siena, Dipartimento di Scienze Fisiche, della Terra e dell'Ambiente<br>Lupetti, Pietro; Università degli Studi di Siena, Dipartimento di Scienze della Vita<br>Magnani, Agnese; Università degli Studi di Siena, Dipartimento di Biotecnologie, Chimica e Farmacia<br>Santucci, Annalisa; Università degli Studi di Siena, Dipartimento di Biotecnologie, Chimica e Farmacia |
| Key Words: | ochronosis, mesoporosity, heat capacity, glycosaminoglycan, rheology |
| | |

# Homogentisic acid induces morphological and mechanical aberration of ochronotic cartilage in alkaptonuria*

Giulia Bernardini[1§], Gemma Leone[1§], Lia Millucci[1], Marco Consumi[1], Daniela Braconi[1], Ottavia Spiga[1], Silvia Galderisi[1], Barbara Marzocchi[1, 4], Cecilia Viti[2], Giovanna Giorgetti[2], Pietro Lupetti[3], Agnese Magnani[1], Annalisa Santucci[1#]

***Running title: Biomechanics of alkaptonuric cartilage***

1 Dipartimento di Biotecnologie, Chimica e Farmacia;

2 Dipartimento di Scienze Fisiche, della Terra e dell'Ambiente;

3 Dipartimento di Scienze della Vita;

Università degli Studi di Siena, via Aldo Moro 2, 53100 Siena, Italy;

4 UOC Patologia Clinica, Azienda Ospedaliera Universitaria Senese, Viale Bracci, Siena, Italy

#Corresponding author: Prof. Annalisa Santucci, Università degli Studi di Siena, Dipartimento di Biotecnologie, Chimica e Farmacia, via Aldo Moro 2, 53100 Siena, Italy, Tel: +390577234958, Fax: +390577234254, E-mail: annalisa.santucci@unisi.it

§ Both authors contributed equally to the paper

**Acknowledgments**

The authors thank the Associazione Italiana Malati di Alcaptonuria (AimAKU) (ORPHA263402), Toscana Life Sciences Orphan_1 project, and FMPS 2008–2010, Dr. Eugenio Paccagnini and Dr. Claudio De Mauro for technical assistance, Prof. Paolo Mariani and Dr. Dario Gambera for providing control cartilage samples.

*In memory of Duccio Calamandrei, a Man of Science and a Friend.

**Abstract**

Alkaptonuria (AKU) is a disease caused by a deficient homogentisate 1,2-dioxygenase activity leading to systemic accumulation of homogentisic acid (HGA), that forms a melanin-like polymer that progressively deposits onto connective tissues causing a pigmentation called "ochronosis" and tissue degeneration. The effects of AKU and ochronotic pigment on the biomechanical properties of articular cartilage need further investigation. To this aim, AKU cartilage was studied by means of thermal (Thermo-gravimetry and Differential Scanning Calorimetry) and rheological analysis. We found that AKU cartilage had a doubled mesopore radius compared to healthy cartilage. Since the mesoporous structure is the main responsible for maintaining a correct hydrostatic pressure and tissue homeostasis, drastic changes of thermal and rheological parameters were found in AKU. In particular, AKU tissue lost its capability to enhance chondrocytes metabolism (decreased heat capacity) and hence the production of proteoglycans. A drastic increase in stiffness and decrease in dissipative and lubricant role ensued in AKU cartilage. Multiphoton and scanning electron microscopies revealed destruction of cell matrix microstructure and disruption of the superficial layer. Such observations on AKU specimens were confirmed in HGA-treated healthy cartilage, indicating that HGA is the toxic responsible of morphological and mechanical alterations of cartilage in AKU.

**Keywords:** ochronosis; mesoporosity; heat capacity; alkaptonuria; glycosaminoglycan; rheology.

**Introduction**

Alkaptonuria (AKU; MIM 203500) is an ultra-rare autosomal recessive metabolic defect, due to an altered structure of homogentisate 1,2-dioxygenase (HGD; E.C.1.13.11.5), an enzyme involved in the metabolism of tyrosine and phenylalanine. Deficiency in HGD activity results in a failure to break down homogentisic acid (HGA), a highly soluble molecule. In AKU, HGA is partly excreted in urine, partly accumulated (plasma levels above 5 μg/mL). Extracellular HGA undergoes oxidation and polymerization causing a dark-brown pigmentation of connective tissues in various organs, a phenomenon known as "ochronosis". The most severe manifestations of AKU occur at the osteoarticular level and include premature severe disabling osteoarthritis-like joint damages, which significantly affect and reduce patient's quality of life (Braconi et al., 2015).

Recently, progresses were made in clarifying the molecular mechanisms and the biochemical pathways playing part in this multisystemic disease (Bernardini et al., 2015; Braconi et al., 2012; Braconi et al., 2011; Braconi et al., 2010a; Braconi et al., 2010b; Laschi et al., 2012; Millucci et al., 2015a; Millucci et al., 2014). Conversely, the damaging effects of ochronosis on the mechanical features of AKU articular cartilage have not been fully investigated. Taylor et al. reported that ochronotic pigmentation starts at the interface with calcified cartilage and then spreads through the deep layers of cartilage and eventually to the articular surface. Therefore, ochronosis should increase the stiffness of extracellular matrix leading to altered stress distribution, further mechanical damage, proliferation of the pigmentation, and a downward spiral of tissue destruction (Taylor et al., 2011).

The main biomechanical function of articular cartilage is to sustain and transmit loads between bones, allowing the joint to have relative motion along multiple axes (Netti and Ambrosio, 2002). From a mechanical viewpoint, the cartilaginous tissue is well characterized and its mechanical /rheological parameters are well known. In particular, since the most relevant loading mode in articular cartilage is dynamic, the time-dependent behaviour has been fully explored. Moreover, the peculiar behaviour of cartilage is strictly related to interstitial fluid movement, which is driven by tissue hydrostatic pressure gradients and is controlled by extracellular matrix (ECM) composition and structure (Netti and Ambrosio, 2002). The ECM comprises about 20% (w/v) of type II collagen arranged to form an elastic fibre network embedded in a gel of large aggregating proteoglycans (Netti and Ambrosio, 2002). Although, the relationship between biomechanics and the structural organization of ECM of cartilage has been extensively investigated both theoretically and experimentally (Varady and Grodzinsky, 2016), our study represents the first report focused on ochronotic cartilage.

In this paper, we analysed the effects of ochronosis on mesostructure, thermal/mechanical behaviour and morphological features of AKU articular cartilage to understand how the deposition of HGA-derived pigment can induce structural alterations. Our findings were also confirmed in an ex vivo cartilage-based AKU model settled up in our laboratory.

## Materials and Methods

### *Cartilage specimens*

Human ochronotic articular cartilage was obtained from three AKU patients who underwent surgery for total knee replacement (Table 1SM). Control cartilage was from age- and gender matched healthy donors who underwent surgery for traumas and did not present any history of rheumatic, osteoarthritis or other degenerative articular diseases. All the procedures were in accordance with the ethical standards of the responsible committee on human experimentation (Comitato Etico Policlinico Universitario di Siena, number GGP10058, date 21/07/2010) and with the Declaration of Helsinki, 1975, as revised in 2000. Informed consent was obtained from all patients.

### *Ex vivo cartilage-based AKU model*

Human articular cartilage samples were dissected under sterile conditions, and cartilage sections were washed in sterile PBS, weighed and placed in 6-well plates. To reproduce the pigmentation of the cartilage observed in AKU, cartilage fragments (five fragments/well) were incubated in DMEM in absence (controls) or in presence of a solution of 0.33 mM HGA for four weeks, up to the development of ochronosis (Tinti et al., 2011). Medium was changed twice a week; conditioned media were collected and conserved at -80°C until biochemical analysis. Histological and biochemical analyses were performed at regular time points (1 week) during the experiments. The experiments were performed in triplicate.

### *Thermal analyses*

Thermogravimetric analysis (TGA): 10-15 mg of cartilage were inserted in a platinum crucible, and heated from RT to 900°C with a heating ramp 10°C/min under nitrogen flow (Leone et al., 2012).

Differential Scanning Calorimetry (DSC) was performed to obtain the following parameters: mesoporosity, ice-melting behaviour and heat capacity of tissues.

Mesoporosity was obtained sealing 10 mg of each sample in aluminium pans and cooling to -60°C. Samples were then heated (5°C $min^{-1}$) and kept to -0.3°C for 10 minutes, and then, cooled down to -60°C with a rate of 0.2°C $min^{-1}$ (Iza et al., 2000). The mesopores radius was calculated applying Eq (1):

$$Rp\ (nm)=(-64.67/\Delta T) + 0.57 \qquad (1)$$

($\Delta T$: shift in the triple point temperature)

The ice-melting behaviour was evaluated cooling samples to -40°C and heating to 40°C with a rate of 2°C $min^{-1}$ (rapid ramp) or 0.2°C $min^{-1}$ (slow ramp) (Leone et al., 2013; Li et al., 2005).

The percentages of water distribution (freezable-$W_{fH,}$ and non-freezable-$W_{nf}$) were determined applying the equation $W_{fH}/W_{ST}=\Delta H_m/\Delta H$, where $W_{ST}$ indicates the total weight of swollen tissue (mg) determined by TGA, $\Delta H_m$ indicates the enthalpy of melting of freezable water (J/g), and $\Delta H$ is the latent heat of water (333.5 J/g) (Li et al., 2005).

The heat capacity was determined as described by McHugh (McHugh et al., 2010) and Abdel-Sayed (Abdel-Sayed et al., 2014). Briefly, the DSC heat flow signals from the sample and the sapphire calibration standard were recorded in the temperature range 10°C-60°C (heating ramp: 10°C $min^{-1}$), and the heat capacity was calculated applying Eq (2) after baseline correction of the flow curves.

$$Cp_{tissues}(T)= (m_{sapphire}/m_{tissue})\cdot[(\varphi_{tissue}(T)- \varphi_0(T))/(\varphi_{sapphire}(T)- \varphi_0(T))]\cdot Cp_{sapphire}(T) \quad (2)$$

(Cp: specific heat capacity; m: mass; φ: DSC output heat flow rate).

***Rheological analyses***

All rheological measurements, i.e. strain sweep analysis, oscillatory shear stress analysis and stress-relaxation analysis, were performed using a controlled strain rheometer.

Fully hydrated samples were placed between two smooth and rigid flat circular plates impermeable to fluid flow in order to reduce dehydration during testing.

Strain sweep test, consisting in monitoring the viscoelastic properties while logarithmically varying the strain amplitude γ0, at a fixed oscillation frequency (0.001Hz, 1Hz and 20Hz), was performed to determine the strain amplitude at which linear viscoelasticity is valid (Mercuri et al., 2008).

Oscillatory shear stress analysis was also performed submitting samples to a sinusoidal angular displacement. A dynamic frequency sweep test was performed with a shear amplitude of $\gamma_0$ =0.01 rad over the physiological frequencies range (0.01-15 Hz) with a 1% strain (Leone et al., 2008a).

Stress-relaxation test was performed imposing increasing strains (5, 20, 30 and 100%) with a relaxation time of 600 s, according to the stress-relaxation time of articular cartilage (Mow et al., 1980). All measurements were performed at 33°C and 37°C.

***Multiphoton microscopy (MPM)***

Two-photon fluorescence (TPF) observations were carried out using a MCube multispot multiphoton microscope (Light4tech, Florence, Italy), equipped with a passive diffractive optical element (DOE) allowing for a degree of parallelization of 16 (4x4 matrix of beamlets) or 64 (8x8 matrix of beamlets). A parallelization approach in excitation and detection was adopted, in order to increase the image frame rate. Detection was achieved by a spatially resolved detector (array of photomultipliers) in descanning optical pathway configuration to minimize the optical cross talk

between different channels when observing scattering tissues. Maximum frame rate was 60 Hz in the 64 beamlets configuration, reduced to about 16 Hz in the 16 beamlets configuration.

***Scanning electron microscopy (SEM)***

Scanning electron microscopy observations were carried out using a Philips1 XL30 device operating at 20 kV. The volume sample analysed, at the actual operating condition, was estimated to have a diameter of ca. 3 µm. The cartilages fragments were carbon coated in order to obtain good quality images under SEM (Lamponi et al., 2012).

***Transmission electron microscopy (TEM)***

Cartilage samples were fixed in 2.5% glutaraldehyde in 0.1 M Cacodylate Buffer (CB) pH 7.2 for 3 h at 4 °C. After rinsing in CB, samples were post-fixed in 1% Osmium Tetroxide in CB for 2 h at 4 °C, dehydrated in a graded series of ethanol and embedded in a mixture of Epon–Araldite resins. Thin sections were stained with uranyl acetate and lead citrate and observed with the TEM FeiTecnai G2 spirit at 80 Kv.

***Collagen staining and quantification***

Cartilage tissue was fixed in 10% formalin for 5 minutes, rinsed with water and then 8-µm thick serial sections were prepared. Pricrosirius Red staining (PSR, Polysciences, Inc) was performed according to manufacturer's instructions. Briefly, cartilage sections were incubated for 90 minutes at RT in the PSR staining solution, rinsed twice with 0.1 N HCl for 1 minute and then once with water, and finally dehydrated in 70% ethanol. Slides were observed under a polarized light microscope (Zeiss Axio Lab.A1).

Conditioned media from cartilage explants cultured in presence of HGA (200 µL) were diluted to 1 mL with PBS, and then incubated with 0.5 mL of chloramine-T solution (50 mM chloramine-T, 30% v/v ethylene glycol monomethyl ether, 50% (v/v) hydroxyproline buffer (0.26 M citric acid, 1.46 M sodium acetate, 0.85 M sodium hydroxide, 1.2% v/v glacial acetic acid), in water) for 20 minutes at RT, followed by 0.5 mL of 3.15 M perchloric acid for 5 minutes at RT. Samples were mixed well after each addition. 0.5 mL of 1.34 M p-dimethylamino-benzaldehyde solution (in ethylene glycol monomethyl ether) was added to each sample and incubated for 20 minutes at 60°C for color development. 4-hydroxy-L-proline was used to generate a standard curve. Standards and samples were read at 557nm on a UV-Vis spectrophotometer. The content of 4-hydroxy-L-proline was normalized to cartilage weight.

***Glycosaminoglycans (GAGs) staining and quantification***

Cartilage sections were stained with Safranin-O/Fast Green staining method (Millucci et al., 2015b), mounted and observed under a light microscope (Zeiss Axio Lab.A1). The dimethylmethylene blue (DMMB) assay was used to quantify GAGs in conditioned medium (Millucci et al., 2012; Tinti et al., 2011). Bovine chondroitin sulphate was used to generate a standard curve. Standards and samples were read at 525 nm on a UV-Vis microplate reader. The content of GAGs was normalized to cartilage weight.

## Results

### *Mesoporus structure and water content of AKU cartilage*

The porosity of cartilage and the percentages of water distribution were determined by TGA and DSC (Figures 1 and 2 ) analysis and reported in Tables 1 and 2. We found that ochronosis caused a significant increase of cartilage porosity (mesopores radius in healthy cartilage: 5.1 ±0.1 nm vs AKU cartilage: 8.8±0.4 nm) (Figure 1a). The total water content in healthy cartilage was about 66.5% whereas in AKU cartilage only about 42.3% respectively (Table 2). Furthermore, by DSC analysis, we were able to discriminate the total water content of each sample into freezable and not-freezable water (i.e. water component that is strictly bound to the proteoglycan chains). We found that the percentage of freezable water was higher in AKU (≈72%) compared to healthy cartilage (≈40%); accordingly, non-freezable water was lower in AKU (≈28%) compared to control (≈60%) (Table 1).

### *Thermal stability of AKU cartilage*

The thermographs of healthy and AKU cartilage, both in native and freeze-dried status, were recorded (Figure 2a and 2b), showing slight differences. The *per cent* of weight losses in three regions of the thermographs were determined and reported in Table 2. As already reported, for samples tested in native status, great difference was observed in the region 30-200 °C relative to total water loss. Another significant difference was seen in terms of R, i.e. the ratio between the weight loss in region 200-400°C, relative to free carbon chain, and the weight loss in region 400-600°C, relative to condensed and more structured carbon component (Leone et al., 2015). The higher the R value, the softer is the matrix. Healthy cartilage showed a R value of 5.1, whereas AKU showed a R value of 4.1 suggesting a more compact structure of the AKU tissue. A similar trend was observed in the freeze-dried samples with R values of 4.6 and 4.2 for healthy and AKU cartilages respectively (Table 2). In addition, in thermographs recorded on freeze-dried status (Figure 2b), AKU samples showed a strict peak centred at about 442°C which was completely absent in thermographs of healthy samples, and that might be related to the decomposition of the melanin-like pigment (Gomez-Marin and Sanchez, 2010). A significant difference was observed in the heat capacity (i.e. self-heating behaviour) of samples, with healthy tissue showing capacity value 5-fold higher (Cp 33°C: 2.9 J/g°C) than AKU (Cp 33°C: 0.5 J/g°C).

### *Mechanical properties of AKU cartilage*

Compressing the tissue of 15%, an average pressure of about 0.5-1 MPa can be simulated representing the contact pressures in the human knee joint (Accardi et al., 2011; Wan et al., 2008). To mimic physiological conditions, a compression of about 15-20% of the thickness of tissues was applied. Samples were allowed to relax before starting with shear test. The mechanical spectra of healthy and AKU cartilage were recorded in the 0.01-15 Hz frequency range,

in order to cover the entire physiological frequency range. Both samples showed a strong 'gel-like' behaviour with the storage modulus (G') greater than the loss modulus (G") of about one order of magnitude within the analysed frequency range (data not shown). Two parameters, i.e. the complex shear modulus, |G*|, and the phase shift angle, δ, were analysed (Figures 3 a and b). The quantity of |G*| provides a measure of the shear stiffness of the tissue under dynamic conditions, while the value of the phase shift angle, δ, is a measure of the dissipation of internal friction (Leone et al., 2008b). The value of shear modulus |G*| for healthy cartilage (0.031± 0.003MPa) was close to values already reported for human tibial cartilage (Wong and Sah, 2010), whereas AKU cartilage showed a higher value all over the frequency range tested (i.e. 0.128± 0.007 MPa). A difference in value of phase shift angle was also observed. In fact, healthy cartilage showed a δ value ranging between 23-11°, whereas AKU cartilage showed a lower δ value all over the frequency range (mean value 7°).

The stress-relaxation behaviour was also analysed, submitting both samples to four different strain percentages (i.e. 5%, 20%, 30% and 100%). Regardless the percentage of strain applied, both samples completely dissipated the stress after just 0.1 s and no significant difference was found in time necessary to dissipate 70% of stress (Table 3). However, a significant difference was observed in the loop test (Figure 3 c). Healthy cartilage showed the characteristic hysteresis area of healthy viscoelastic tissues due to the dissipative component of the tissue, and completely recovered its original modulus. On the contrary, the stress-relaxation curves observed for AKU cartilage confirmed the complete breakdown of the mechanical properties of the tissue (Figure 3 c).

***Morphology of AKU cartilage***

Cartilage auto-fluorescence was assessed by TPF microscopy to evaluate integrity of the ECM network from the surface up to 160 μm of depth. The considerably lower (3-fold) auto-fluorescence of AKU cartilage (Figure 4), indicated a reduced ECM density respecting to healthy cartilage that, on the contrary, exhibited only a faint attenuation of fluorescence intensity throughout the image depth (160 μm) (Figure 4 a-b). TPF analysis also indicated that surface structure of AKU cartilage was more fibrous and rough than healthy cartilage, which, conversely, appeared smooth and isotropic. This was consistent with macroscopic results due to increased friction between joint surfaces, wear and algetic exposure upon using the joint, which are typical symptoms of ochronotic osteoarthritis. As observed in the 50 μm z-stack, AKU cartilage revealed also microscopic internal lesions (arrow in Figure 4 d) and the fibrillation of the ECM where the diagonally oriented fibrils altered the intensity of native fluorescence. These observations confirmed the degraded state of AKU tissue since in healthy cartilage (Moger et al., 2007) the network of elastin fibres was found lying parallel to the articular surface in the most superficial 50 μm of the tissue.

Consistent with the findings from TPF analysis, SEM investigation revealed distinct differences in surface ultrastructure between AKU and healthy articular cartilage (Figure 5 a-h). In control cartilage, surface appeared smooth and the matrix surrounding chondrocytes was uniform with a layer of collagen fibers leaning parallel to the articular surface. In these specimens, chondrocytes werw regular in shape and individually located into well appreciable lacunae (black arrowhead in Figure 4 b-d). In AKU, samples the presence of a sheet like collagen network was noted. The collagen bands appeared as separate structures and no cells were observable in the layers. Several defects on AKU cartilage surface were distinguishable such as vertically oriented flatter incisions (French brackets in Figure 5 e-h), as well as rounded concave defects where the ochronotic pigment was deposited and surrounded by a thick mound (arrows in Figure 5 f). The size of these peculiar oblong areas corresponds to chondrocytes size and represent the empty lacunae of degenerated cells. Some collagen fibers appeared to emerge from the tissue surface sheet and some chondrons (white arrowhead Figure 5 h) were clearly visible suggesting a dramatic damage occurred to the tissue.

TEM analysis confirm the disruption of ECM ultrastructure and chondrocytes degeneration in ochronotic tissue. AKU cartilage (Figure 1 SM) showed a disorganized net of broken collagen fibres; sparse pigment deposits were clearly visible and were supposed to be responsible for the fragmentation and of the lack of periodicity of collagen fibres. AKU chondrocytes showed typical features of chondroptosis (Millucci et al., 2015b): strong shrinking, self-destruction through autophagic vacuoles and blebbing with disruption of the cellular membrane and organelles.

***HGA induced destruction of ECM network in an ex vivo AKU cartilage model***

To confirm the role of HGA on the ECM integrity, we performed PSR and Safranin-O/Fast Green staining in histological sections of cartilage explants maintained for 1 month in a growth medium containing HGA 0.33 mM (Figure 6 a-f).

The distribution of the orange-red birefringence in AKU cartilage model indicated that the zonal boundaries and orientation of collagen fibrils was not as expected. Large patches of birefringence scattered throughout the tissue with no well-defined borders, in particular in the superficial zone (SZ) and in the tidemark (TM) were observed. Orientation of collagen fibrils boundles was random and the perpendicularity of the fibres totally lost, indicating advanced tissue degeneration (arrows).

In the overall, these results suggested that isotropic changes in the collagen fibers occurred in both the superficial and deep zones of AKU cartilage model. On the contrary, in healthy cartilage crimping of the collagen fibrils was evident. Moreover, as expected, collagen fibrils in SZ were densely packed and had a highly ordered alignment parallel to the articular surface and perpendicular to collagen fibrils in the transitional zone (TZ).

Safranin-O staining was used to detect changes in proteoglycans content (Figure 6 b). In AKU specimens, a general variability in proteoglycan distribution was observed across the section, with more intensely stained areas near the surface and faintly discoloured areas towards the calcified zone. In AKU model, surface discontinuity was evident: SZ was fractured and severely pigmented. Large incisions extended throughout the transitional/deep zone. Cartilage matrix loss was observed looking at the augmented area of the tidemark (Figure 6 b, arrows). On the contrary, surface of healthy cartilage was smooth, the matrix components and chondrocytes were well organized and distributed throughout the whole tissue.

Finally, to evaluate the degree of cartilage degradation due to HGA, we measured the release of hydroxyproline residues and GAGs in conditioned medium (Figure 6 g-h). An enhanced released of both hydroxyproline and GAGs was found in HGA-treated tissue, suggesting that HGA might mediate cartilage degeneration. Interestingly, the release of GAGs was exponential during the first two weeks of culture, with a fold change relative to control > 2; later, a severe reduction was observed (last two weeks) (Figure 6 h).

**Discussion**

There are major limitations in studying the alkaptonuric ochronosis. AKU is a very rare disease and research surrounding the mechanism of disease progression has highlighted that HGA-based pigment accumulation covers time lasting decades.

To enable a better understanding of the pathophysiology involved in the progression of ochronosis and the related osteoarthropathy, we have characterized the articular cartilage from AKU patients and healthy controls, using thermal, rheological and in depth ultrastructural analysis. To the best of our knowledge, this study is the first to evaluate similar changes in AKU cartilage giving a comprehensive view of the mechanical and structural properties of the tissue.

The peculiar behaviour and function of articular cartilage is a direct consequence of its micro- and mesostructure that, ensuring the correct movement and distribution of the interstitial fluid through the matrix interfibrillar space (2–6 nm), regulates tissue homeostasis and biomechanical properties (Netti and Ambrosio, 2002). In particular, mesostructure and the total amount of interstitial fluid depend on the collagen-proteoglycans network, where the dense collagen network restricts the hydration of these molecules to 40-60% generating the correct swelling pressure to ensure the compressive stiffness of cartilage (Leone, 2011).

Cartilage tissue degeneration (Millucci et al., 2017;Mitri et al., 2017), chronic inflammation (Braconi et al., 2015; Millucci et al., 2015a; Millucci et al., 2015b; Millucci et al., 2012), and ochronotic arthropathy (Millucci et al., 2017) (Geminiani et al., 2017) are the main and most severe manifestations of AKU. Both the high affinity of HGA for collagenous tissue and the ability of chondrocytes to accumulate this metabolite promote ochronotic pigment deposition

in joints and thus the rapid onset of ochronotic arthropathy (Laschi et al., 2012). Ultrastructural analysis of AKU cartilage revealed that collagen fibres were covered with ochronotic pigment deposits that altered the periodicity of collagen fibres leading to loss of tissue architecture (Millucci et al., 2012; Taylor et al., 2011; Taylor et al., 2010). Moreover, amyloid aggregates were found in AKU cartilage co-localizing with the ochronotic pigment (Millucci et al., 2015b; Millucci et al., 2012). The co-presence of amyloid and ochronotic pigment deposits associated to collagen fibres could affect the correct ratio between collagen and proteoglycans, and alter the role of collagen in regulating the swelling of the hydrophilic component of the network.

In this work, we found that ochronotic AKU cartilage presented with a doubled diameter pores, suggesting drastic alterations of the hydrostatic pressure of tissue and a decreased load-bearing capacity. This might also suggest in turn an altered trafficking of nutrients and waste within the matrix AKU (Vikingsson et al., 2015). We also found that proteoglycan content was markedly reduced in AKU cartilage. Several lines of evidence demonstrated that the decrease of proteoglycans in AKU cartilage is due to the action of proteoglycan-degrading enzymes (Millucci et al., 2015b) and/or to the inadequate synthesis and released of proteoglycans by AKU chondrocytes (Tinti et al., 2010). Here, we confirmed that GAGs release is significantly increased in HGA-treated samples, suggesting that in vivo cartilage undergoes significant degeneration due to HGA action. Alterations of cartilage micro- and mesostructures in AKU might have important and detrimental effects also on chondrocytes physiology, in particular in mechanosensing and mechanoresponse processes (Gambassi et al., 2016; Thorpe et al., 2017). AKU chondrocytes suffer from a particular form of programmed cell death, named chondroptosis (Millucci et al., 2015b), and severe aberrations of the cytoskeleton were observed in AKU chondrocytes as well as in HGA-treated chondrocytes (Braconi et al., 2012; Geminiani et al., 2017), with important consequences for chondrogenesis and cell differentiation, but also for the synthesis and release of the ECM components, in particular collagen and proteoglycans, and for the responsiveness of chondrocytes to the external mechanical stimuli (Geminiani et al., 2017). Structural disorganization of chondrocytes primary cilium (length reduction) was also demonstrated in AKU as well as in HGA-treated chondrocytes and associated to an activation of the Hedgehog pathway (Gambassi et al., 2016; Thorpe et al., 2017).

Our results also demonstrate that AKU cartilage lost its self-heating behaviour (decrease of heat capacity) and this phenomenon can be a relevant player in osteoarticular manifestation of the disease. In fact, the ability of normal articular cartilage to locally increase its temperature by dissipating part of the mechanical energy into heat is fundamental to enhance chondrocytes metabolism and cartilage homeostasis in terms of ECM components production and release (Abdel-Sayed et al., 2014; Abdel-Sayed et al., 2013). As reported, cartilage degeneration and loss of its viscoelastic properties greatly reduce the heat capacity of the tissue and is associated with a significant loss of GAGs (Abdel-Sayed et al., 2014).

The decrease of the viscous or dissipative component of the tissue deeply affects the mechanical and frictional responses of AKU cartilage to compressive strain (Accardi et al., 2011; Wan et al., 2008). Differences in terms of shear modulus |G*| and phase shift angle indicate a dramatic increase of the shear stiffness of AKU tissue. As reported, compressive stiffness is also increased in AKU cartilage, where pigmented AKU cartilage shows a Young's modulus 5 fold higher (156 MPa) compared to non-pigmented or osteoarthritis tissues (22.4 and 26.3 MPa respectively), revealing that such a difference is due to pigment deposition (Taylor et al., 2011). In addition, stress-relaxation behaviour of AKU cartilage indicates a relevant loss of resilience, which is the capability of tissues to undergo loads without cracking. Fragmentation of degenerated ochronotic cartilage is well documented in AKU arthropathy (Di Franco et al., 2000; Millucci et al., 2012; Taylor et al., 2011). These fragments, namely ochronotic shards, were found embedded in the synovium or in the in the marrow cavity, surrounded by fibrous tissue, multinucleated giant and macrophagic cells. Moreover, such important alterations in AKU cartilage biomechanical properties might also reflect on osteoblast/osteoclast phenotype and on the homeostasis and signalling of bone tissue, leading to an abnormal bone remodelling and to the formation of trabecular excrescences (Taylor et al., 2012; Taylor et al., 2011).

In order to assess the severity of a pathology or the efficacy of regenerative treatments, the accurate characterization of articular cartilage morphology is crucial. This is why we undertook TPF and SEM analyses, which pointed out AKU cartilage surface and subsurface abnormalities consisting of degradation of proteoglycans with unmasking and fragmentation of collagen fibrillar network. If the surface of healthy cartilage was slightly undulated, that of AKU was scattered with pits, elevations and depressions indicative of significant tissue damage. This finding suggests that the continuous deposition of ochronotic pigment leads to a progressive delamination of AKU cartilage causing the appearance of superficial, deep craters.

In conclusion, we demonstrated that the presence of ochronosis affects the physico-thermal and mechanical properties of AKU cartilage. Although the exact mechanism of cartilage degradation in AKU is not fully clarified, our results suggest that HGA could affect collagen molecules, proteoglycans moiety and chondrocytes homeostasis (Geminiani et al., 2017; Millucci et al., 2015b; Millucci et al., 2012; Taylor et al., 2011; Taylor et al., 2010; Tinti et al., 2010), not only triggering, but also accelerating and amplifying the degenerative processes in AKU cartilage (Taylor et al., 2017). Our observations support an interdependent relationship between mechanical and biochemical matrix degradation resulting in peculiar lesions of AKU cartilage. This process, once triggered, is progressive and irreversible, and the reparative responses, if present, are not sufficient or adequate to restore tissue functionality.

Our study, combining rheological and ultrastructural analyses, can also offer interesting perspectives for the development of novel therapies for AKU, and provide diagnostic tools able to detect AKU specific features (especially in young, asymptomatic patients), monitor disease progression and response to treatments.

**Compliance with Ethics Guidelines**

All procedures followed were in accordance with the ethical standards of the responsible committee on human experimentation (institutional and national) and with the Helsinki Declaration of 1975, as revised in 2000 (5). Informed consent was obtained from all patients for being included in the study.

**Conflict of Interest**

Giulia Bernardini, Gemma Leone, Lia Millucci, Marco Consumi, Daniela Braconi, Ottavia Spiga, Silvia Galderisi, Barbara Marzocchi, Cecilia Viti, Giovanna Giorgetti, Pietro Lupetti, Agnese Magnani and Annalisa Santucci declare that they have no conflict of interest.

**References**


Abdel-Sayed P, Moghadam MN, Salomir R, Tchernin D, Pioletti DP. 2014. Intrinsic viscoelasticity increases temperature in knee cartilage under physiological loading. Journal of the Mechanical Behavior of Biomedical Materials 30:123-130.

Abdel-Sayed P, Vogel A, Moghadam MN, Pioletti DP. 2013. Cartilage Self-Heating Contributes to Chondrogenic Expression. European Cells & Materials 26:171-178.

Accardi MA, Dini D, Cann PM. 2011. Experimental and numerical investigation of the behaviour of articular cartilage under shear loading-Interstitial fluid pressurisation and lubrication mechanisms. Tribology International 44(5):565-578.

Bernardini G, Laschi M, Geminiani M, Braconi D, Vannuccini E, Lupetti P, Manetti F, Millucci L, Santucci A. 2015. Homogentisate 1,2 dioxygenase is expressed in brain: implications in alkaptonuria. Journal of inherited metabolic disease 38(5):807-814.

Braconi D, Bernardini G, Bianchini C, Laschi M, Millucci L, Amato L, Tinti L, Serchi T, Chellini F, Spreafico A, Santucci A. 2012. Biochemical and proteomic characterization of alkaptonuric chondrocytes. Journal of cellular physiology 227(9):3333-3343.

Braconi D, Bianchini C, Bernardini G, Laschi M, Millucci L, Spreafico A, Santucci A. 2011. Redox-proteomics of the effects of homogentisic acid in an in vitro human serum model of alkaptonuric ochronosis. Journal of inherited metabolic disease 34(6):1163-1176.

Braconi D, Laschi M, Amato L, Bernardini G, Millucci L, Marcolongo R, Cavallo G, Spreafico A, Santucci A. 2010a. Evaluation of anti-oxidant treatments in an in vitro model of alkaptonuric ochronosis. Rheumatology (Oxford, England) 49(10):1975-1983.

Braconi D, Laschi M, Taylor AM, Bernardini G, Spreafico A, Tinti L, Gallagher JA, Santucci A. 2010b. Proteomic and redox-proteomic evaluation of homogentisic acid and ascorbic acid effects on human articular chondrocytes. Journal of cellular biochemistry 111(4):922-932.

Braconi D, Millucci L, Bernardini G, Santucci A. 2015. Oxidative stress and mechanisms of ochronosis in alkaptonuria. Free radical biology & medicine 88(Pt A):70-80.

Di Franco M, Coari G, Bonucci E. 2000. A morphological study of bone and articular cartilage in ochronosis. Virchows Arch 436(1):74-81.

Gambassi S, Geminiani M, Thorpe SD, Bernardini G, Millucci L, Braconi D, Orlandini M, Thompson CL, Petricci E, Manetti F, Taddei M, Knight MM, Santucci A. 2016. Smoothened-antagonists reverse homogentisic acid-induced alterations of Hedgehog signaling and primary cilium length in alkaptonuria. Journal of cellular physiology.

Geminiani M, Gambassi S, Millucci L, Lupetti P, Collodel G, Mazzi L, Frediani B, Braconi D, Marzocchi B, Laschi M, Bernardini G, Santucci A. 2017. Cytoskeleton Aberrations in Alkaptonuric Chondrocytes. Journal of cellular physiology 232(7):1728-1738.

Gomez-Marin AM, Sanchez CI. 2010. Thermal and mass spectroscopic characterization of a sulphur-containing bacterial melanin from Bacillus subtilis. Journal of Non-Crystalline Solids 356(31-32):1576-1580.

Iza M, Woerly S, Danumah C, Kaliaguine S, Bousmina M. 2000. Determination of pore size distribution for mesoporous materials and polymeric gels by means of DSC measurements: thermoporometry. Polymer 41(15):5885-5893.

Lamponi S, Leone G, Consumi M, Greco G, Magnani A. 2012. In vitro biocompatibility of new PVA-based hydrogels as vitreous body substitutes. Journal of biomaterials science Polymer edition 23(1-4):555-575.

Laschi M, Tinti L, Braconi D, Millucci L, Ghezzi L, Amato L, Selvi E, Spreafico A, Bernardini G, Santucci A. 2012. Homogentisate 1,2 dioxygenase is expressed in human osteoarticular cells: implications in alkaptonuria. Journal of cellular physiology 227(9):3254-3257.

Leone G. 2011. Cartilage replacement implants using hydrogels. Biomedical Hydrogels: Biochemistry, Manufacture and Medical Applications:149-183.

Leone G, Bidini A, Lamponi S, Magnani A. 2013. States of water, surface and rheological characterisation of a new biohydrogel as articular cartilage substitute. Polymers for Advanced Technologies 24(9):824-833.

Leone G, Consumi M, Lamponi S, Magnani A. 2012. New hyaluroran derivative with prolonged half-life for ophthalmogical formulation. Carbohydrate Polymers 88(3):799-808.

Leone G, Delfini M, Di Cocco ME, Borioni A, Barbucci R. 2008a. The applicability of an amidated polysaccharide hydrogel as a cartilage substitute: structural and rheological characterization. Carbohydrate Research 343(2):317-327.

Leone G, Torricelli P, Chiumiento A, Facchini A, Barbucci R. 2008b. Amidic alginate hydrogel for nucleus pulposus replacement. Journal of Biomedical Materials Research Part A 84A(2):391-401.

Leone G, Volpato MD, Nelli N, Lamponi S, Boanini E, Bigi A, Magnani A. 2015. Continuous multilayered composite hydrogel as osteochondral substitute. Journal of Biomedical Materials Research Part A 103(8):2521-2530.

Li WB, Xue F, Cheng RS. 2005. States of water in partially swollen poly(vinyl alcohol) hydrogels. Polymer 46(25):12026-12031.

McHugh J, Fideu P, Herrmann A, Stark W. 2010. Determination and review of specific heat capacity measurements during isothermal cure of an epoxy using TM-DSC and standard DSC techniques. Polymer Testing 29(6):759-765.

Mercuri D, Leone G, Barbucci R, Favaloro R, Facchini A, Signori F, Bronco S, Ciardelli E. 2008. An artificial disc: Chemical and biomechanical analysis. Macromol Symp 266:74-80.

Millucci L, Bernardini G, Spreafico A, Orlandini M, Braconi D, Laschi M, Geminiani M, Lupetti P, Giorgetti G, Viti C, Frediani B, Marzocchi B, Santucci A. 2017. Histological and Ultrastructural Characterization of Alkaptonuric Tissues. Calcified tissue international 101(1):50-64.

Millucci L, Braconi D, Bernardini G, Lupetti P, Rovensky J, Ranganath L, Santucci A. 2015a. Amyloidosis in alkaptonuria. Journal of inherited metabolic disease 38(5):797-805.

Millucci L, Ghezzi L, Paccagnini E, Giorgetti G, Viti C, Braconi D, Laschi M, Geminiani M, Soldani P, Lupetti P, Orlandini M, Benvenuti C, Perfetto F, Spreafico A, Bernardini G, Santucci A. 2014. Amyloidosis, inflammation, and oxidative stress in the heart of an alkaptonuric patient. Mediators of inflammation 2014:258471.

Millucci L, Giorgetti G, Viti C, Ghezzi L, Gambassi S, Braconi D, Marzocchi B, Paffetti A, Lupetti P, Bernardini G, Orlandini M, Santucci A. 2015b. Chondroptosis in alkaptonuric cartilage. Journal of cellular physiology 230(5):1148-1157.

Millucci L, Spreafico A, Tinti L, Braconi D, Ghezzi L, Paccagnini E, Bernardini G, Amato L, Laschi M, Selvi E, Galeazzi M, Mannoni A, Benucci M, Lupetti P, Chellini F, Orlandini M, Santucci A. 2012. Alkaptonuria is a novel human secondary amyloidogenic disease. Biochimica et biophysica acta 1822(11):1682-1691.

Mitri E, Millucci L, Merolle L, Bernardini G, Vaccari L, Gianoncelli A, Santucci A. 2017. A new light on Alkaptonuria: A Fourier-transform infrared microscopy (FTIRM) and low energy X-ray fluorescence (LEXRF) microscopy correlative study on a rare disease. Biochimica et biophysica acta 1861(5 Pt A):1000-1008.

Moger CJ, Barrett R, Bleuet P, Bradley DA, Ellis RE, Green EM, Knapp KM, Muthuvelu P, Winlove CP. 2007. Regional variations of collagen orientation in normal and diseased articular cartilage and subchondral bone determined using small angle X-ray scattering (SAXS). Osteoarthritis and cartilage 15(6):682-687.

Mow VC, Kuei SC, Lai WM, Armstrong CG. 1980. Biphasic creep and stress relaxation of articular cartilage in compression? Theory and experiments. Journal of biomechanical engineering 102(1):73-84.

Netti PA, Ambrosio L. 2002. Articular Cartilage. In: Barbucci R, editor. Integrated Biomaterials Science. Boston, MA: Springer US. p 381-402.

Taylor AM, Boyde A, Davidson JS, Jarvis JC, Ranganath LR, Gallagher JA. 2012. Identification of trabecular excrescences, novel microanatomical structures, present in bone in osteoarthropathies. Eur Cell Mater 23:300-308; discussion 308-309.

Taylor AM, Boyde A, Wilson PJ, Jarvis JC, Davidson JS, Hunt JA, Ranganath LR, Gallagher JA. 2011. The role of calcified cartilage and subchondral bone in the initiation and progression of ochronotic arthropathy in alkaptonuria. Arthritis and rheumatism 63(12):3887-3896.

Taylor AM, Hsueh MF, Ranganath LR, Gallagher JA, Dillon JP, Huebner JL, Catterall JB, Kraus VB. 2017. Cartilage biomarkers in the osteoarthropathy of alkaptonuria reveal low turnover and accelerated ageing. Rheumatology (Oxford, England) 56(1):156-164.

Taylor AM, Wlodarski B, Prior IA, Wilson PJ, Jarvis JC, Ranganath LR, Gallagher JA. 2010. Ultrastructural examination of tissue in a patient with alkaptonuric arthropathy reveals a distinct pattern of binding of ochronotic pigment. Rheumatology (Oxford, England) 49(7):1412-1414.

Thorpe SD, Gambassi S, Thompson CL, Chandrakumar C, Santucci A, Knight MM. 2017. Reduced primary cilia length and altered Arl13b expression are associated with deregulated chondrocyte Hedgehog signaling in alkaptonuria. Journal of cellular physiology 232(9):2407-2417.

Tinti L, Spreafico A, Braconi D, Millucci L, Bernardini G, Chellini F, Cavallo G, Selvi E, Galeazzi M, Marcolongo R, Gallagher JA, Santucci A. 2010. Evaluation of antioxidant drugs for the treatment of ochronotic alkaptonuria in an in vitro human cell model. Journal of cellular physiology 225(1):84-91.

Tinti L, Spreafico A, Chellini F, Galeazzi M, Santucci A. 2011. A novel ex vivo organotypic culture model of alkaptonuria-ochronosis. Clinical and experimental rheumatology 29(4):693-696.

Varady NH, Grodzinsky AJ. 2016. Osteoarthritis year in review 2015: mechanics. Osteoarthritis and cartilage 24(1):27-35.

Vikingsson L, Claessens B, Gomez-Tejedor JA, Gallego Ferrer G, Gomez Ribelles JL. 2015. Relationship between micro-porosity, water permeability and mechanical behavior in scaffolds for cartilage engineering. J Mech Behav Biomed Mater 48:60-69.

Wan LQ, Jiang J, Arnold DE, Guo XE, Lu HH, Mow VC. 2008. Calcium Concentration Effects on the Mechanical and Biochemical Properties of Chondrocyte-Alginate Constructs. Cellular and molecular bioengineering 1(1):93-102.

Wong BL, Sah RL. 2010. Mechanical asymmetry during articulation of tibial and femoral cartilages: Local and overall compressive and shear deformation and properties. Journal of Biomechanics 43(9):1689-1695.

**Figure legends:**

**Figure 1:** DSC melting and solidification profile of healthy (HC) and diseased AKU cartilages (DC) (a). DSC melting profile of frozen completely swollen healthy (HC) and AKU cartilages (DC) heating ramp 2°C/min (b). More resolved melting peaks were obtained decreasing the heating ramp (slow ramp 0.2°C/min) allowing to discriminate total water content into freezable water and not-freezable water (c). The AKU and healthy tissues showed a superimposable melting profile with two peaks located at identical temperature being the lowest due to not-freezable water and the highest to freezable water.

**Figure 2:**TG thermographs obtained plotting the derivative of weight *versus* temperature of healthy (HC) and AKU cartilages (DC), and recorded on sample in native state (d), or on freeze-dried samples (e).

**Figure 3:** Complex Modulus |G*| (a) and δ values (b) of healthy (HC) and AKU cartilages (DC) recorded at 37°C in the entire physiological range of frequencies (0.01-15Hz). Complex Moduli |G*| of healthy (HC) and AKU cartilage (DC) as function of increasing strain (0% -100% strain) and decreasing strain (0% -100% strain) (c)**.** All the measurements were performed at 33°C (rest temperature) and 37°C (working temperature). No difference was observed, so only results at 37°C were plotted.

**Figure 4:** 3D reconstruction of native TPF of human healthy (a) and AKU (b) cartilage. Microscopic lesions are visible at the articular surface of AKU cartilage. The size of the reconstruction is 210x 210 x 160 µm. Greyscale represents relative fluorescence intensity in arbitrary units where the highest is white and lowest is black. TPF images from a single-image plane within a z-stack, corresponding to 5 0 µm in depth from the surface, from both healthy (c) and AKU (d) samples. Z-stack images of the AKU samples showed the presence of cracks within the ECM (arrow). Cracks were not observed in control samples.

**Figure 5:** SEM imaging of the surface of healthy (a-d) and AKU cartilage (e-h). Ultrastructural features of most damaged region of AKU cartilage showing extensive fissuring of tissue (French brakets). Surface of healthy articular cartilage appears smooth with no superficial lesions, cracks or fissures (a), lacunae containing chondrocytes are indicated (black arrowheads). Significant fissures and fibrillations can be seen in AKU cartilage images (b), which depict the rough surface of severely degenerated cartilage, empty lacunae (white arrowhead) and rounded concave defects (arrows) are indicated. (scale bar 10 µm for a, b, e, f and g; scale bar 20 µm for c and h; scale bar 50 µm for d).

**Figure 6:** Representative images of Picrosirius Red staining of longitudinal cross sections of control (a and c) and AKU model cartilage (b and d). Images were acquired in bright (a and b) and polarized (c and d) light. Explicative areas indicating collagen fiber alignment are indicated (arrows). Representative images of Safranin-O and Fast Green staining of longitudinal cross sections of control (e) and AKU (f) model cartilage. Thickness of tidemark is indicated. Magnification 10X; SZ: superficial zone; TZ: transitional/deep zone; TM: tidemark.

Hydroxiproline assay of conditioned media from cartilage explants cultured in presence of HGA (g). A progressive collagen degradation in the first two weeks of treatment was observed. *p<0.05, **p<0.01, ***p<0.001, ****p<0.0001; Student's t-test.

DMMB assay of conditioned media from cartilage explants cultured in presence of HGA (h). An increase in GAGs release in the first two weeks of treatment was observed. *p<0.05, **p<0.01, ***p<0.001, ****p<0.0001; Student's t-test.

**Captions Supplementary Figures**

**Figure 1 SM:** TEM observation of AKU cartilage. The presence of aggregates of amyloid fibrils is detectable between broken collagen fibrils, finally sprinkled with pigment drop-like granules (bar 25 μm).

**Table 1:** Non-freezing water, bound freezing water and bulk freezing water determined by DSC for healthy cartilage (HC) and diseased cartilage (DC) (n = 3).

| Sample | TGA | | DSC | WfH/WSG= ΔHm/ ΔH | |
|---|---|---|---|---|---|
| | WST[#] | WH[a] | ΔHm[b] | WfH[c] | Wnf[e] |
| HC | 5.1±0.2 | 3.39±0.02 | 105.3±0.3 | 1.36±0.03 (40±1%)[d] | 2.03±0.01 (60±2%)[f] |
| DC | 10.8±0.4 | 4.57±0.04 | 94.3±0.9 | 3.30±0.05 (72±2%)[d] | 1.26±0.02 (28±1%)[f] |
| water | / | / | 332.4±0.1* | / | / |

[#:] weight of total swollen tissue (mg) determined by TGA

[a:] total water (mg) determined by heating each sample determined by TGA in the temperature range:30-200°C.

/: no data

[b]: enthalpy of melting (J/g); [*]: latent heat (frozen water) (J/g);

[c]: freezing water (mg); [d]: percentage of freezing water obtained following the procedure reported by Li, et al (Li et al., 2005).

[e]: not freezing water (mg) [f]: percentage of not freezing water obtained following the procedure reported by Li, et al (Li et al., 2005).

**Table 2:** TGA/DTG analysis of native and freeze-dried samples (Healthy Cartilage: HC; Diseased Cartilage: DC): Weight loss in 30-120°C temperature range: free water; Weight loss in 120-200°C range: hydration water; Weight loss in 30-200°C temperature range: free and hydration water; 200-400°C: free carbon chains; 400-600°C: condensed and more structured carbon component; R: stiffness index: 200-400/400-600; Weight loss in 30-900°C range: total loss. Data were reported as % mean value (n=3)

| Sample | 30-120°C | 120-200°C | 30-200°C | 200-400°C | 400-600°C | R | 30-900°C |
|---|---|---|---|---|---|---|---|
| Native | | | | | | | |
| HC | 55.8±0.6 | 10.7±0.5 | 66.5±0.7 | 20.3±0.6 | 3.97±0.03 | 5.1±0.3 | 98.6±0.9 |
| DC | 36.8±0.4 | 5.54±0.05 | 42.3±0.2 | 30.4±0.5 | 7.44±0.03 | 4.1±0.2 | 95.4±0.6 |
| Freeze-dried | | | | | | | |
| HC | 6.02±0.02 | 7.51±0.5 | 13.5±0.3 | 50.6±0.7 | 11±1 | 4.6±0.3 | 97.1±0.6 |
| DC | 6.08±0.03 | 6.38±0.5 | 12.5±0.7 | 46.4±0.8 | 11±1 | 4.2±0.1 | 86.5±0.5 |

**Table 3**: Stress-relaxation values for healthy tissue (HC) and diseased tissue (DC) at different strain percentage (n = 3)

| | Strain | Peak max (MPa) | 70% [#] | Relaxation % after 0.1s | Relaxation % after 500s |
|---|---|---|---|---|---|
| HC | 5% | 0.007±0.001 | 0.0046±0.0001 | 96.3±0.5 | 99.1±0.2 |
| | 20% | 0.031±0.004 | 0.0046±0.0001 | 95.6±0.3 | 99.4±0.1 |
| | 30% | 0.044±0.003 | 0.0046±0.0001 | 95.7±0.4 | 99.5±0.2 |
| | 100% | 0.090±0.001 | 0.0066±0.0001 | 95.5±0.2 | 99.7±0.3 |
| DC | 5% | 0.020±0.001 | 0.0046±0.0001 | 91.0±0.2 | 96.5±0.2 |
| | 20% | 0.064±0.002 | 0.0056±0.0001 | 92.0±0.1 | 96.5±0.3 |
| | 30% | 0.086±0.003 | 0.0056±0.0001 | 94.5±0.3 | 97.3±0.2 |
| | 100% | 0.090±0.001 | 0.0077±0.0001 | 96.5±0.2 | 98.1±0.1 |

[#]: time (s) necessary to reach 70% of relaxation

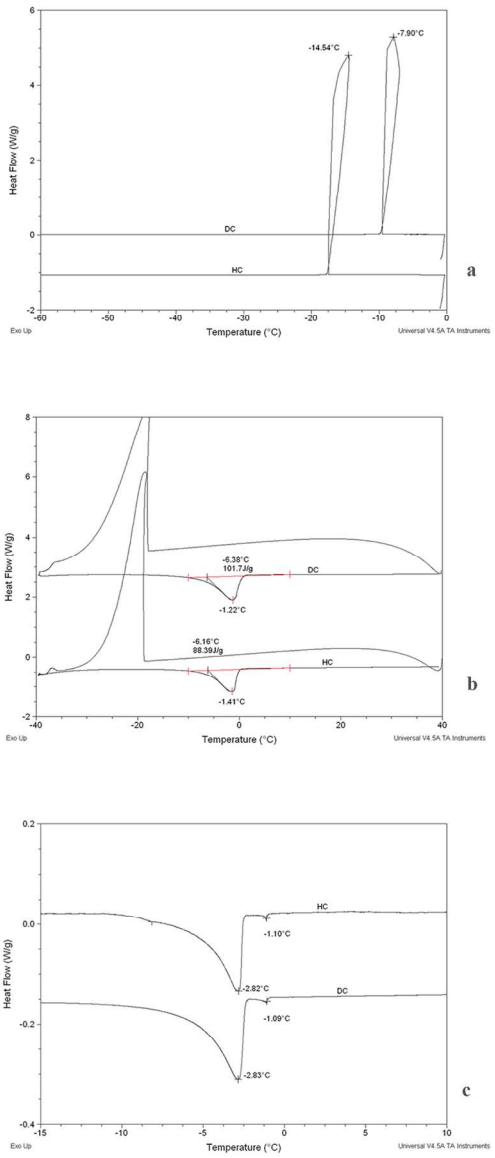


**Figure 1**

209x297mm (300 x 300 DPI)

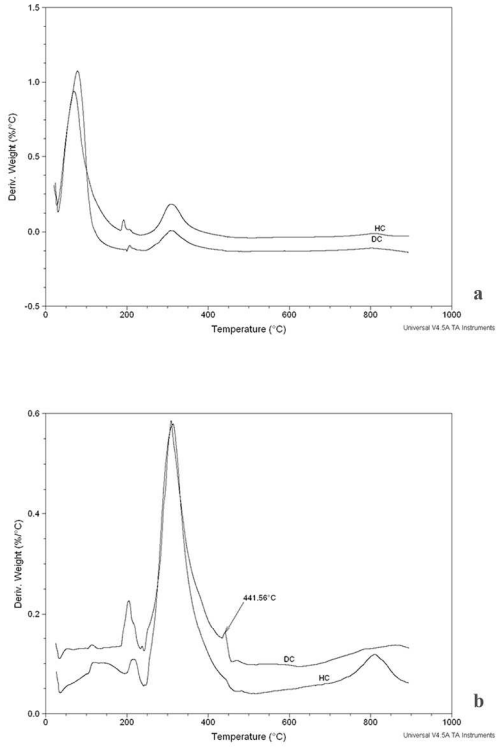


**Figure 2**

209x297mm (300 x 300 DPI)

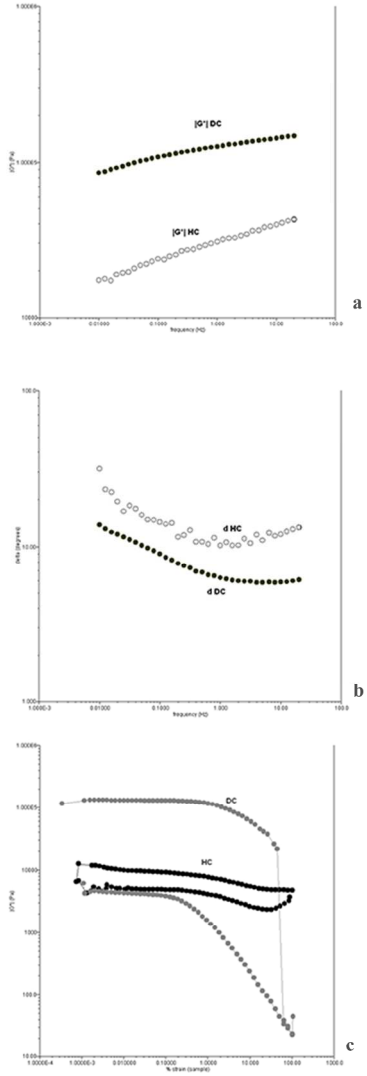


**Figure 3**

209x297mm (300 x 300 DPI)

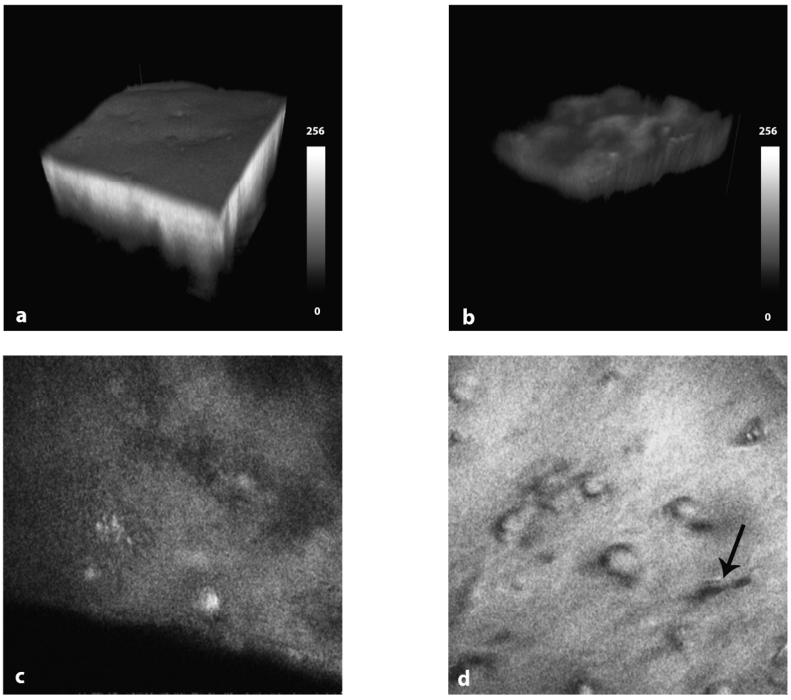


160x120mm (299 x 299 DPI)

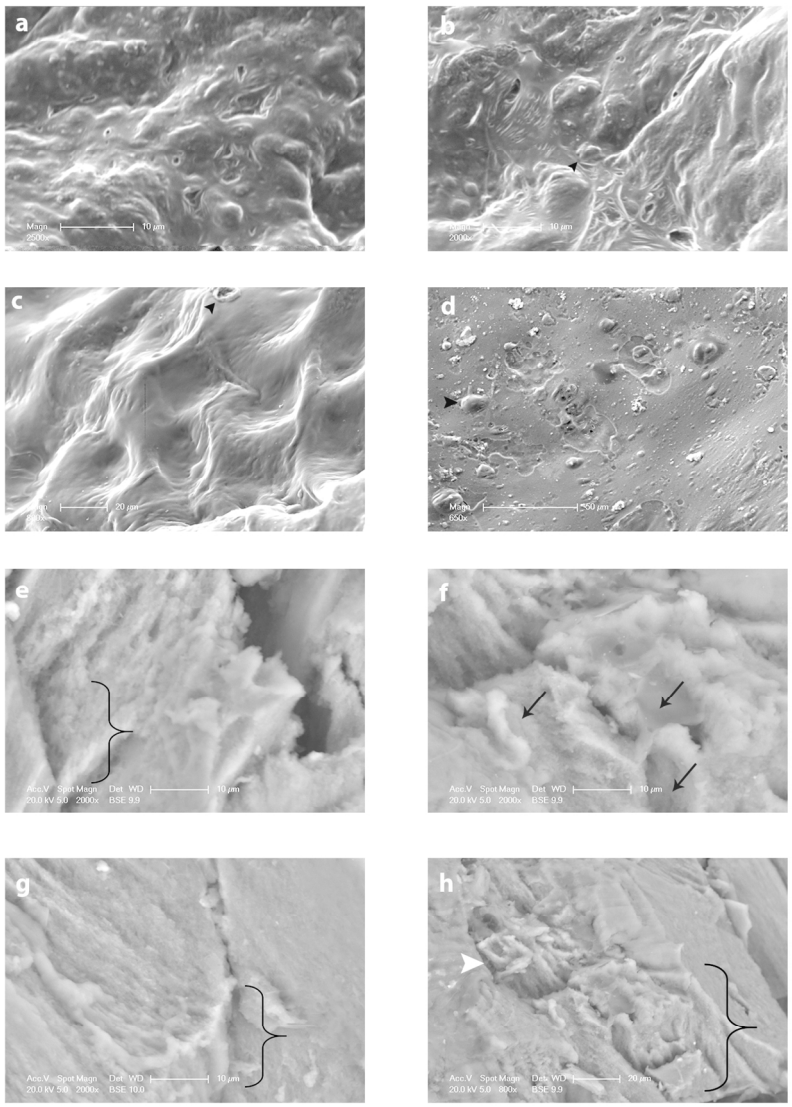


119x160mm (300 x 300 DPI)

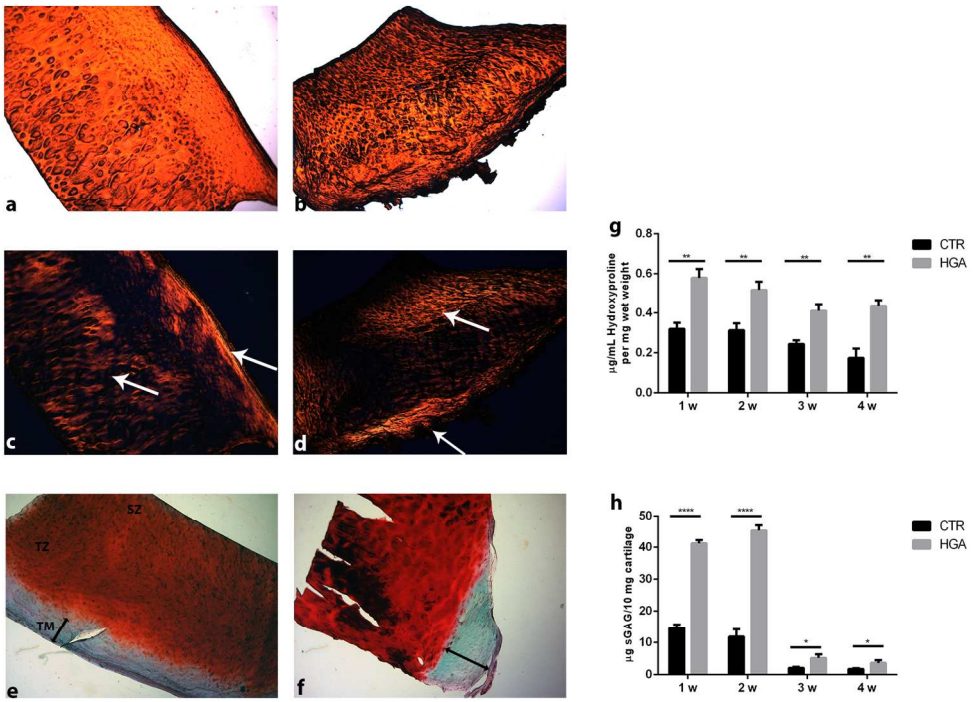


160x120mm (299 x 299 DPI)